

Deep Learning for Detecting Cerebral Aneurysms with CT Angiography



Jiehua Yang, MS* • Mingfei Xie, MD* • Canpei Hu, MS • Osamah Alwalid, MD • Yongchao Xu, PhD • Jia Liu, MD • Teng Jin, PhD • Changde Li, MBBS • Dandan Tu, PhD • Xiaowu Liu, PhD • Changzheng Zhang, MS • Cixing Li, MS • Xi Long, PhD

From the School of Electronic Information and Communications, Huazhong University of Science and Technology, South 1st Building, Luoyu Road 1037, Wuhan 430074, China (J.Y., C.H., Y.X.); Department of Radiology, Union Hospital, Tongji Medical College, Huazhong University of Science and Technology, Wuhan, China (M.X., O.A., J.L., T.J., X. Long); Hubei Province Key Laboratory of Molecular Imaging, Wuhan, China (M.X., O.A., J.L., T.J., X. Long); Department of Radiology, Xin Cai People's Hospital, Xin Cai, China (Changde Li); and Huawei Technologies, Shenzhen, China (D.T., X. Liu, C.Z., Cixing Li). Received September 21, 2019; revision requested November 12; final revision received July 10, 2020; accepted September 10. Address correspondence to X. Long (e-mail: xilong@hust.edu.cn).

*J.Y. and M.X. contributed equally to this work.

Conflicts of interest are listed at the end of this article.

See also the editorial by Kallmes and Erickson in this issue.

Radiology 2020; 00:1–10 • <https://doi.org/10.1148/radiol.2020192154> • Content codes:  

Background: Cerebral aneurysm detection is a challenging task. Deep learning may become a supportive tool for more accurate interpretation.

Purpose: To develop a highly sensitive deep learning–based algorithm that assists in the detection of cerebral aneurysms on CT angiography images.

Materials and Methods: Head CT angiography images were retrospectively retrieved from two hospital databases acquired across four different scanners between January 2015 and June 2019. The data were divided into training and validation sets; 400 additional independent CT angiograms acquired between July and December 2019 were used for external validation. A deep learning–based algorithm was constructed and assessed. Both internal and external validation were performed. Jackknife alternative free-response receiver operating characteristic analysis was performed.

Results: A total of 1068 patients (mean age, 57 years \pm 11 [standard deviation]; 660 women) were evaluated for a total of 1068 CT angiograms encompassing 1337 cerebral aneurysms. Of these, 534 CT angiograms (688 aneurysms) were assigned to the training set, and the remaining 534 CT angiograms (649 aneurysms) constituted the validation set. The sensitivity of the proposed algorithm for detecting cerebral aneurysms was 97.5% (633 of 649; 95% CI: 96.0, 98.6). Moreover, eight new aneurysms that had been overlooked in the initial reports were detected (1.2%, eight of 649). With the aid of the algorithm, the overall performance of radiologists in terms of area under the weighted alternative free-response receiver operating characteristic curve was higher by 0.01 (95% CI: 0.00, 0.03).

Conclusion: The proposed deep learning algorithm assisted radiologists in detecting cerebral aneurysms on CT angiography images, resulting in a higher detection rate.

© RSNA, 2020

Online supplemental material is available for this article.

Cerebral aneurysms are causative for about 80%–90% of nontraumatic subarachnoid hemorrhages (1,2), with a mortality rate of 23%–51% (1,3) and a 10%–20% risk of permanent disability (4). The risk of aneurysm rupture depends on the size, shape, and location of the aneurysm (5). Therefore, the detection and characterization of cerebral aneurysms are critical for management guidance.

CT angiography is usually the first-line imaging examination for evaluating cerebral aneurysms (6), with high reported sensitivity and specificity of up to 98% and 100%, respectively (2). Compared with MR angiography, CT angiography is a fast and cost-effective diagnostic technique with usually wider availability and high spatial resolution. Compared with digital subtraction angiography, CT angiography is usually more widely available and is noninvasive (7,8).

Deep learning is a branch of machine learning that is increasingly used to develop algorithms for image recognition (9). In radiology, deep learning has been applied recently in several assisting roles, such as assessment of bone age on radiographs of the hand in pediatric populations (10), detection of tuberculosis on chest radiographs (11), automated detection of cerebral aneurysms at MR angiography (12), prioritization in radiologic workflow and reduction of time to diagnosis of intracranial hemorrhage on nonenhanced CT images (13), and detection of pulmonary nodules on chest CT images (14,15). Computer-aided investigation of acute neurologic disorders in neuroimaging may play a role in the triage of radiologic workflow, resulting in shorter time to treatment and improved management outcomes (16).

Because of the small size of cerebral aneurysms and the complexity of intracranial vessels, cerebral aneurysms may

Abbreviation

wAFROC = weighted alternative free-response receiver operating characteristic

Summary

Deep learning for detection of cerebral aneurysms with CT angiography enhances radiologists' performance by facilitating aneurysm detection and reducing the number of overlooked aneurysms.

Key Results

- The proposed algorithm detected cerebral aneurysms on CT angiographic images with a sensitivity of 97.5% (633 of 649 aneurysms).
- Of 649 aneurysms, the algorithm detected eight (1.2%) new aneurysms (at false-positive rate per case of 13.8) that were missed in the initial radiologic reports.
- With the help of the algorithm, the overall performance of radiologists in detection of cerebral aneurysms was increased by 0.01 (from 0.60 to 0.61).

be overlooked during the initial assessment. Double reading decreases the false-negative rate of aneurysm detection to 1% (2). The development of a supportive algorithm that assists in the detection of cerebral aneurysms may be beneficial for both patients and physicians.

In this study, we aimed to develop a fully automated, highly sensitive algorithm that can be used for detection of cerebral aneurysms on CT angiography images.

Materials and Methods

The study protocol was approved by our institutional review board; written informed consent was waived because this was a retrospective study of preexisting imaging data.

Data Acquisition

Inclusion criteria included availability of head or head and neck CT angiography images with at least one radiologically reported untreated intracranial aneurysm, regardless of age, indication, clinical manifestation, and morphologic features. Images with severe motion artifacts were excluded. The images were consecutively retrieved from the imaging databases of two hospitals of Huazhong University of Science and Technology (Union Hospital and Union West Hospital) and were acquired with four different scanners between January 2015 and June 2019. Images from each scanner were divided equally and randomly between training and validation sets. An additional 400 CT angiograms acquired between July and December 2019 were used for external validation. The imaging protocol included standard CT angiography of the head or head and neck with variable imaging parameters (Table E1 [online]).

Development of the Algorithm

CT angiograms with reported intracranial aneurysms were used to develop and assess the algorithm. A three-dimensional detection algorithm based on a convolutional neural network was developed. All images were rescaled to a spacing of $0.39 \times 0.39 \times 0.39$ mm³. During training, the rescaled images were cropped to $128 \times 128 \times 128$ pixels and then fed

into a one-stage detector as described previously (17). Convolutional block attention module (18) was added into Res-block of ResNet-18 (19); moreover, dense atrous convolution and residual multikernel pooling blocks (20) were used between encoding and decoding stages (Fig E1 [online]).

For testing, the trained algorithm was used to predict the probability of aneurysm existence and the size at each voxel and to draw a bounding box on the feature suspected to be an aneurysm. Those locations with high probabilities were selected as candidates. The overlapped candidates were then filtered out by using nonmaximum suppression.

Hyperparameters were selected by using fivefold cross-validation on the training set. During training, a stochastic gradient descent optimizer with a learning rate of 0.01 and weight decay of 10^{-4} was used. The algorithm converged after 100 epochs. The threshold of overlap in nonmaximum suppression was set to 0.02. All images were automatically preprocessed with SimpleITK version 1.2.0 (<http://www.simpleitk.org>), and the detector was implemented by using Pytorch framework 0.4.1 (<https://pytorch.org>). Code is available at <https://github.com/CTA-detection/DLCA>.

Evaluation of the Algorithm

Two general radiologists (X. Long and M.X.) with 7 and 5 years of experience in CT angiography of the head, respectively, independently annotated the aneurysms by using software (3D Slicer version 4.10.1; <https://www.slicer.org>). Reference standard for diagnosis included, in addition to the radiologic report (by at least two of 49 radiologists with 3–23 years of experience in CT angiography of the head, three of whom are authors X. Long, M.X., and J.L.), a careful independent read by each of the two radiologists who performed the annotation. Any disagreement was solved by discussion and consensus between the two annotating radiologists.

Two radiologists (X. Long and M.X.) reviewed the algorithm predictions on the validation set and evaluated the result of the aneurysm recall.

Both internal and external validation were performed. In internal validation, 100 CT angiograms positive for aneurysms and extracted from the validation set were interpreted by four general radiologists (T.J., J.L., M.X., and X. Long) of different experience levels (3, 3, 5, and 7 years for radiologists 1 through 4, respectively) without and with algorithm assistance. External validation was carried out by four general radiologists (with 1, 3, 5, and 7 years of experience in CT angiography of the head) who were blinded to the clinical indication, radiologic reports, and other imaging examinations. Random samples of 200 of the 400 CT angiograms were assigned to each of the four radiologists for random interpretation either with or without aid of the algorithm. Following a 2-week washout period, the same selected sample was randomly interpreted again by the same corresponding radiologist without or with aid of the algorithm (if the first read was with algorithm aid, then the second read was without algorithm aid, and vice versa). The aneurysm type, number, location, and size and time to diagnosis were recorded for each interpreted image.

Table 1: Characteristics of 1068 Patients and 1337 Aneurysms Included in Algorithm Development

Feature	Union Hospital			Union West Hospital
	GE	Siemens	Toshiba	Philips
No. of CT angiograms	440	283	251	94
No. of men (total, 408)	180	97	96	35
No. of women (total, 660)	260	186	155	59
Mean age (y)	56 ± 10	57 ± 11	56 ± 11	61 ± 11
Men	55 ± 9	55 ± 13	56 ± 12	56 ± 12
Women	57 ± 10	57 ± 10	56 ± 11	63 ± 10
No. of aneurysms	577	321	324	115
Aneurysm type				
Saccular	548	307	306	114
Fusiform	29	14	18	1
Mean size of aneurysms (mm)	5.6 ± 3.5	5.3 ± 4.6	4.5 ± 3.2	5.6 ± 3.0
Aneurysm size				
<3 mm	100	65	107	18
3–5 mm	188	153	129	35
5–10 mm	246	77	70	54
>10 mm	43	26	18	8
Aneurysm location				
Internal carotid artery	234	239	212	74
Middle cerebral artery	111	40	46	19
Anterior cerebral artery	52	14	17	6
Anterior communicating artery	86	14	12	8
Posterior communicating artery	35	4	12	3
Posterior cerebral artery	12	2	7	2
Vertebral artery	14	6	7	1
Basilar artery	28	1	6	2
Other locations	5	1	5	0

Note.—Unless otherwise specified, data are numbers of patients or numbers of aneurysms. Mean data are ± standard deviation.

Statistical Analysis

The proposed algorithm was evaluated on the validation set by calculating its sensitivity and free-response receiver operating characteristic curve. Difference between recalled and nonrecalled groups in patients' sex, number of aneurysms, aneurysm type, and aneurysm location was tested by using χ^2 test, and the difference in age and mean aneurysm size was tested by using t test.

On the external validation set, the jackknife alternative free-response receiver operating characteristic analysis was performed with freely available software (JAFROC, version 4; <http://www.devchakraborty.com>) with a random-readers and random-cases model (21). By considering the clinical importance of each lesion, the area under weighted alternative free-response receiver operating characteristic (wAFROC) curve on the basis of equal weight for each lesion in multiple-lesion CT angiograms was used to assess the overall performance of readers. Multilevel generalized linear models were used for comparing the performance among repeated measures. Multilevel linear models were used to evaluate the time to diagnosis of readers. Descriptive statistical analysis was performed by using GLIMMIX, MIXED, and LOGISTIC procedures in SAS software (version 9.4; SAS Institute, Cary NC), and confidence intervals of proportions were calculated by using the Clopper-Pearson method. P values less than .05 were considered to indicate a statistically significant result.

Results

Patient and Cerebral Aneurysm Characteristics

After exclusion of CT angiograms with no aneurysms ($n = 8187$) and those with severe motion artifact ($n = 7$), 1068 CT angiograms encompassing 1337 cerebral aneurysms from 1068 patients (mean age, 57 years ± 11 [standard deviation]; 660 women) were used for algorithm development. CT angiograms were acquired with four different scanners, including Discovery CT750 HD (GE Healthcare, Chicago, Ill; $n = 440$), Somatom Definition AS+ (Siemens Healthineers, Erlangen, Germany; $n = 283$), and Aquilion ONE (Toshiba, Tokyo, Japan; $n = 251$) at Union Hospital and Ingenuity CT scanner (Philips Healthcare, Best, the Netherlands; $n = 94$) at Union West Hospital. The detailed characteristics of patients and aneurysms are listed in Table 1. The flowchart of data acquisition, selection, and division are presented in Figure 1.

The training set involved 688 cerebral aneurysms from 534 patients. Of these, 197 were men (age range, 7–90 years; mean age, 55 years ± 12), and 337 were women (age range, 21–89 years; mean age, 58 years ± 11). The size of aneurysms ranged from 1.2 mm to 45.6 mm, with a mean size of 5.3 mm ± 3.9. The training set contained 649 saccular aneurysms and 39 fusiform aneurysms.

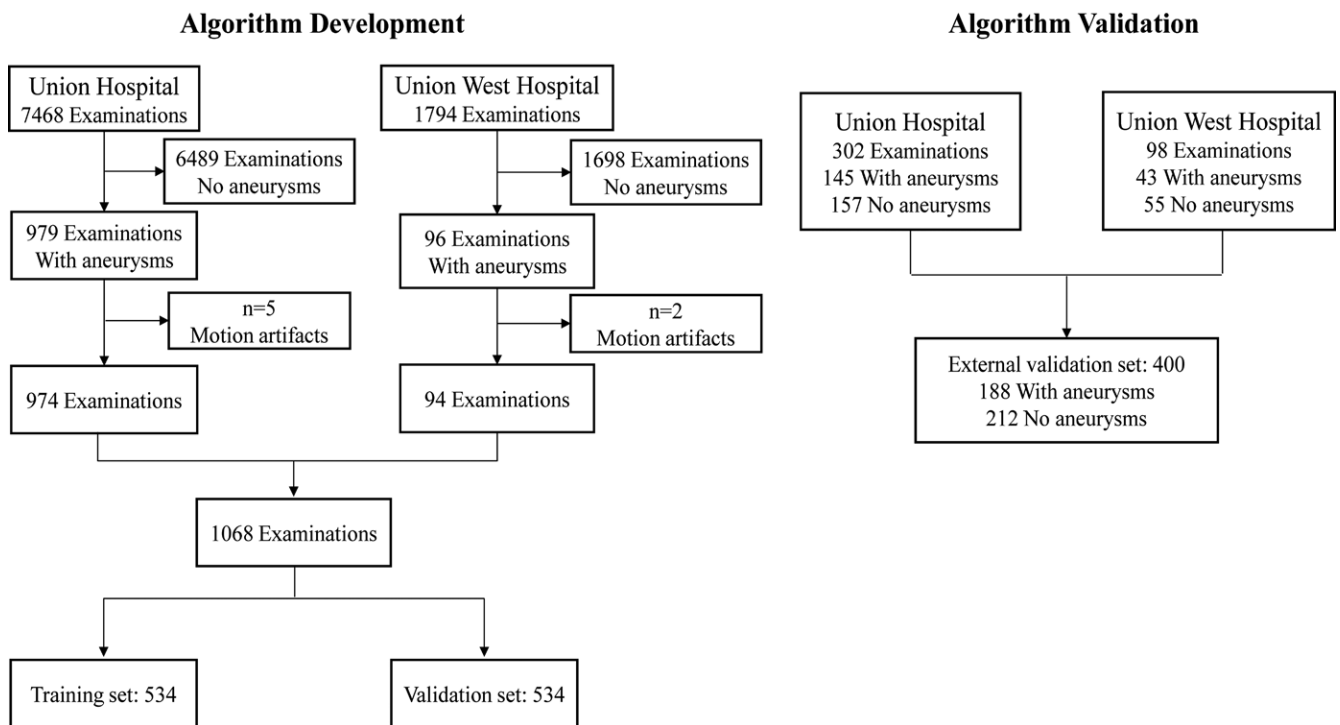


Figure 1: Flowchart of data acquisition, selection, and division.

In the validation set, there were 649 cerebral aneurysms from 534 patients, including 211 men (age range, 10–83 years; mean age, 56 years \pm 10) and 323 women (age range, 25–93 years; mean age, 57 years \pm 10). The size of aneurysms ranged from 1.2 mm to 30.8 mm (mean size, 5.2 mm \pm 3.6). There were 626 saccular aneurysms and 23 fusiform aneurysms.

The external validation set involved an extra 400 CT angiograms that were acquired from the same two hospitals (Union Hospital, $n = 302$; Union West Hospital, $n = 98$) with the same four scanners (GE Healthcare, $n = 101$; Siemens, $n = 99$; Toshiba, $n = 102$; and Philips, $n = 98$). Of the 400 CT angiograms, there were 188 CT angiograms that were positive for aneurysms, encompassing 206 aneurysms in 66 male patients (age range, 29–85 years; mean age, 59 years \pm 11) and 122 female patients (age range, 31–86 years; mean age, 59 years \pm 10). The size of aneurysms ranged from 1 mm to 22 mm (mean size, 4.1 mm \pm 2.6). There were 193 saccular aneurysms and 13 fusiform aneurysms. The characteristics of the training, validation, and external validation sets are provided in Table 2.

Algorithm Performance

The training and validation sets and results of aneurysm recall on the validation set are given in Table 2. The maximum sensitivity of aneurysm detection by using the proposed algorithm was 97.5% (633 of 649; 95% CI: 96.0, 98.6), with a rate of false-positive findings per case of 13.8. The free-response receiver operating characteristic curve is shown in Figure 2. Representative images with false-positive findings are illustrated in Figure 3.

Nonrecalled aneurysms were mostly smaller than 3 mm in longest diameter and found near the bony structures. Typical examples are shown in Figure 4. The performance of the developed algorithm stratified according to the type, size, and location of aneurysm and the imaging scanner is presented in Table 2. The sensitivities of detection of saccular aneurysms and fusiform aneurysms were 97.6% (611 of 626; 95% CI: 96.1, 98.7) and 95.7% (22 of 23; 95% CI: 78.1, 99.9), respectively. The algorithm performance showed a gradual improvement in sensitivity regarding aneurysm size, reaching 100% (49 of 49) in aneurysms 10 mm or larger. In terms of location, the lowest sensitivity was observed in aneurysms located on the anterior and posterior cerebral arteries; however, most of these aneurysms were smaller than 3 mm.

There was no difference between recalled and nonrecalled aneurysm groups in patients' sex ($P = .74$), age ($P = .30$), aneurysm type ($P = .44$), aneurysm location ($P = .16$), or scanner type ($P = .76$). However, there was a difference in aneurysm size between the two groups ($P < .01$; Table 2).

The annotating radiologists found eight newly discovered aneurysms that had been overlooked during the initial reporting. Among these, six aneurysms were smaller than 3 mm and two were in the size range of 3–5 mm. Three of these aneurysms were located on the basilar artery, two were located on the internal carotid artery, and the other three aneurysms were distributed on the anterior cerebral artery, posterior cerebral artery, and posterior communicating artery. Typical examples of these aneurysms are shown in Figure 5.

Table 2: Characteristics of Training, Validation Including Results of Aneurysms Recall, and External Validation Sets

Characteristic	Training Set	Validation Set			External Validation Set	
		Total	Recalled	<i>P</i> Value*	Positive Findings	Negative Findings
No. of CT angiograms	534	534	525 (98.3) [96.8, 99.2]	...	188	212
Sex74
No. of men	197	211	207 (98.1) [95.2, 99.5]	...	66	141
No. of women	337	323	318 (98.5) [96.4, 99.5]	...	122	71
Mean age (y)	57 ± 11	56 ± 1030	59 ± 10	56 ± 12
Men	55 ± 12	56 ± 10	59 ± 11	56 ± 13
Women	58 ± 11	57 ± 10	59 ± 10	54 ± 12
No. of aneurysms	688	649	633 (97.5) [96.0, 98.6]	...	206	
Aneurysm type44
Saccular	649	626	611 (97.6) [96.1, 98.7]	...	193	...
Fusiform	39	23	22 (95.7) [78.1, 99.9]	...	13	...
Mean size of aneurysms (mm)	5.3 ± 3.9	5.2 ± 3.6	4.1 ± 2.6	...
Aneurysm size001
<3 mm	155	135	125 (92.6) [86.8, 96.4]	...	69	...
3–5 mm	242	263	258 (98.1) [95.6, 99.4]	...	85	...
5–10 mm	245	202	201 (99.5) [97.3, 100]	...	43	...
>10 mm	46	49	49 (100) [92.8, 100]	...	9	...
Aneurysm location16
Internal carotid artery	397	362	352 (97.2) [95.0, 98.7]	...	119	...
Middle cerebral artery	118	98	97 (99.0) [94.5, 100]	...	31	...
Anterior cerebral artery	44	45	41 (91.1) [78.8, 97.5]	...	7	...
Anterior communicating artery	55	65	65 (100) [94.5, 100]	...	25	...
Posterior communicating artery	29	25	25 (100) [86.3, 100]	...	8	...
Posterior cerebral artery	10	13	12 (92.3) [64.0, 99.8]	...	4	...
Vertebral artery	13	15	15 (100) [78.2, 100]	...	6	...
Basilar artery	16	21	21 (100) [83.9, 100]	...	5	...
Other locations	6	5	5 (100) [47.8, 100]	...	1	...
Scanner distribution of aneurysms76
GE Discovery CT750 HD	297	280	274 (97.9) [95.4, 99.2]	...	51	50
Siemens Definition AS+	162	159	156 (98.1) [94.6, 99.6]	...	46	53
Toshiba Aquilion ONE	172	152	147 (96.7) [92.5, 98.9]	...	48	54
Philips Ingenuity CT	57	58	56 (96.6) [88.1, 99.6]	...	43	55

Note.—Unless otherwise specified, data are numbers of patients or numbers of aneurysms, with percentages in parentheses; numbers in brackets are 95% CIs of the percentages. Mean data are ± standard deviation.

* *P* value of difference between recalled and nonrecalled aneurysm groups.

Algorithm Validation

Results of radiologists' performance in image interpretation without and with algorithm assistance in internal validation are presented in Table E2 (online). In external validation, 400 new CT angiograms (188 positive findings and 212 negative findings) were individually interpreted by four radiologists without and with the aid of the algorithm. Table 3 lists the results of external validation at each individual level. The overall areas under the wAFROC curve without and with algorithm aid were 0.60 and 0.61, respectively. The difference was 0.01 (95% CI: 0.00, 0.03). Sensitivity per lesion without and with algorithm aid was 79.09% and 88.94%, respectively. The difference was 9.85% (95% CI: 4.92, 14.79). Sensitivity per case without and with algorithm aid was 81.63% and 91.86%, respectively. The difference was 10.23% (95% CI: 5.48, 15.00). Specificity per case without and with algorithm aid was 95.94%

and 90.93%, respectively. The difference was −5.01% (95% CI: −8.35, −1.68). Time to diagnosis was slightly lower (difference, −3.62 seconds; 95% CI: −9.85, 2.59); however, this difference was not statistically significant. In particular, the area under the wAFROC curve for radiologists 1 and 2, with less experience, improved by 0.03 (95% CI: 0.00, 0.06) and 0.02 (95% CI: 0.00, 0.04), respectively, with aid of the algorithm. For the wAFROC plot of each reader, see Figure E2 (online). For detailed results of the performance and comparisons, as well as the estimates of multilevel generalized linear models of radiologists' performance and the estimates of multilevel linear models for reading time, see Tables E3–E7 (online) and Figure E3 (online).

Discussion

Cerebral aneurysms are causative for the majority of subarachnoid hemorrhages, yet detection of cerebral aneurysms

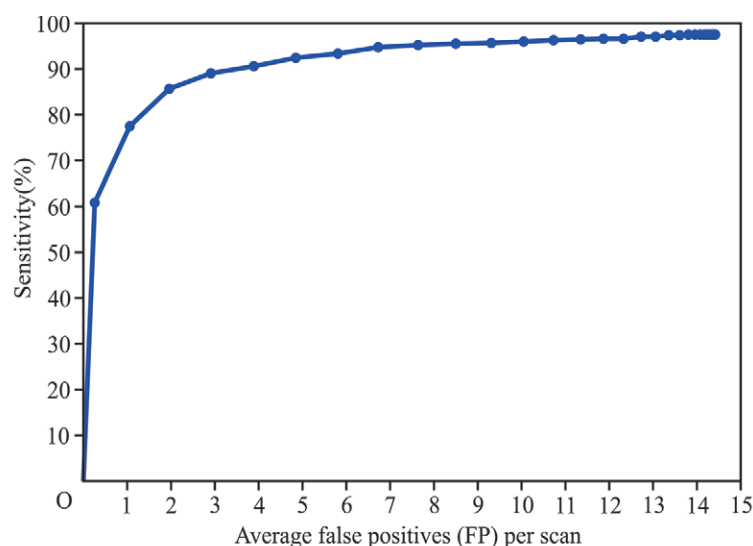


Figure 2: Free-response receiver operating characteristic curve of algorithm performance on validation set.

remains challenging (1,3). In our study, we used deep learning to develop a supportive algorithm to assist radiologists in detecting cerebral aneurysm on CT angiograms. The sensitivity of detection of cerebral aneurysms with use of the developed algorithm was as high as 97.5% (633 of 649). The developed algorithm revealed eight new aneurysms that were overlooked in the initial reports. With aid of the proposed algorithm, the overall performance in terms of area under the weighted alternative free-response receiver operating characteristic (wAFROC) curve of radiologists improved by 0.01 ($P < .05$). This improvement was found to be dependent on the level of experience.

The application of deep learning in detection of cerebral aneurysm has been mostly performed on MR angiography images. Sichtermann et al (22) developed and assessed an algorithm and achieved an overall sensitivity of 90%. A computer-assisted detection system on the basis of deep learning was also proposed by Nakao et al (23) and attained a sensitivity of 94.2% (98 of 104). In another study, Ueda et al (12) developed an algorithm to detect cerebral aneurysms with a sensitivity of 93% on MR angiography images obtained with MRI scanners from different vendors and at various facilities. The sensitivity of their algorithm in large aneurysms with diameters of 5.0–9.9 mm and 10 mm or greater was 86% and 83% compared with 99.5% and 100% in our study, respectively. The relatively limited sensitivity for large aneurysms was attributed to the heterogeneous internal signal of the large aneurysms at MR angiography.

There are fewer studies on detection of aneurysm with deep learning in CT angiography. In a study conducted by Vaseemahmed et al (24), a sensitivity of 100% was achieved for detection of cerebral aneurysms on CT angiography images. However, the generalizability of this algorithm needs to be proven because it was assessed with only six aneurysms.

Recently, Park et al (6) proposed a deep learning method to assist radiologists in diagnosing cerebral aneurysms at CT angiography. They conducted an experiment by using 328 CT angiography images with aneurysms and 490 CT angiography images without aneurysms. They observed an improvement in the sensitivity, specificity, accuracy, and time to diagnosis in interpretation of 59 images with aneurysms and 56 images without aneurysms. However, their experimental data did not include aneurysms smaller than 3 mm, which are more likely to be overlooked by radiologists and require more time to be diagnosed. Furthermore, the aforementioned study (6) did not include cases of subarachnoid hemorrhage or patients with surgical devices in situ.

Our data included images from patients with subarachnoid hemorrhage caused by ruptured aneurysms, as these patients are at a higher risk of future aneurysm rupture (2,7). It also included aneurysms smaller than 3 mm and patients with surgical devices in situ.

On external validation, the overall performance of radiologists in aneurysm detection improved with algorithm aid (area under wAFROC curve, 0.01; $P < .05$) in our study. This improvement was most pronounced for the two least experienced radiologists (areas under wAFROC curve, 0.03 and 0.02; $P < .05$) compared with the two more experienced radiologists (areas under wAFROC curve, 0.01 and 0.01; $P > .05$). This indicates a greater benefit of the algorithm to less experienced radiologists. Similarly, Miki et al (25) also proved feasibility of an MR angiography-based computer-assisted detection system.

There were a number of limitations in our study. First, the retrospective collection of the study data may have introduced a spectrum bias. Second, although the algorithm assisted radiologists in locating cerebral aneurysms, it was unable to provide accurate information about the aneurysm shape, which is among

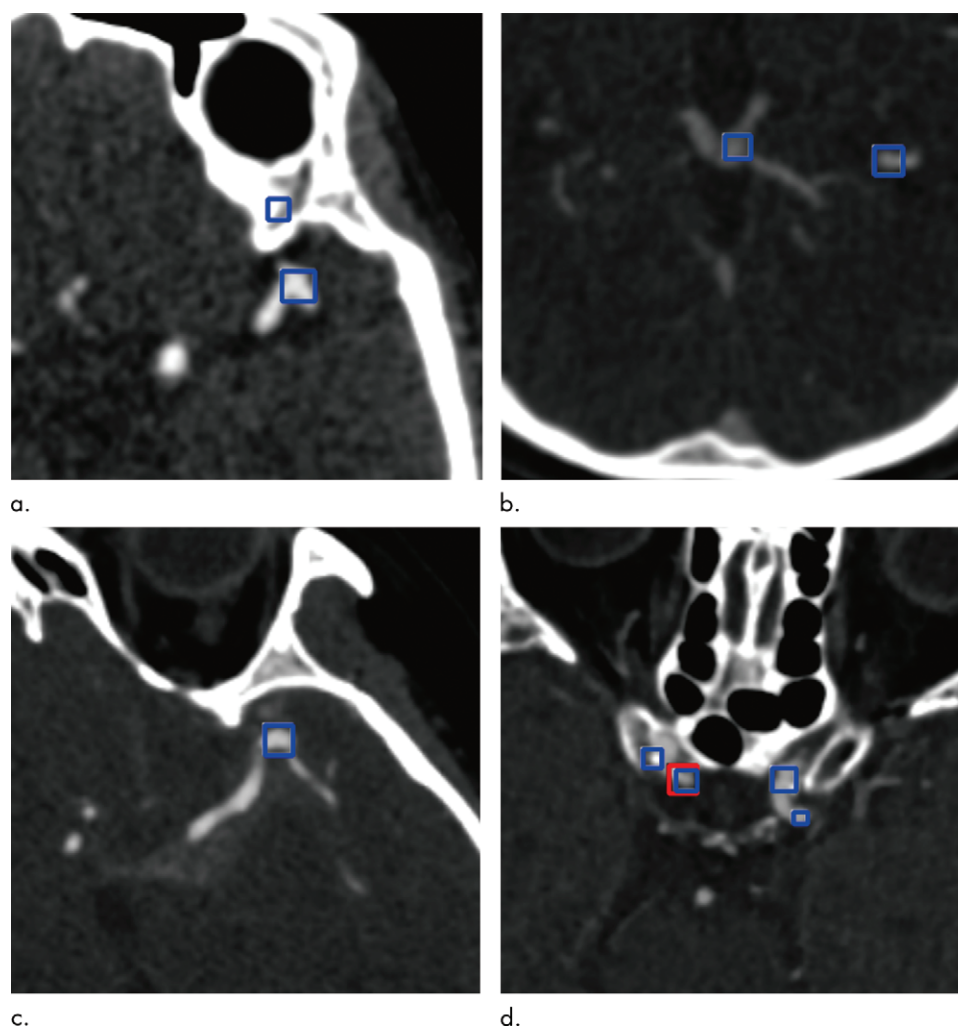


Figure 3: Images show examples of false-positive aneurysms, including (a) bony structures and vessel bifurcation, (b) veins, (c) vessel curvatures, and (d) calcified plaques. Red box (d) indicates aneurysms annotated by radiologists, and the blue boxes indicate aneurysm candidates provided by the algorithm.



Figure 4: Images in a 54-year-old woman with aneurysm 2.9 mm in maximum diameter located on left internal carotid artery (arrow). (a) Axial section head CT angiogram and (b) volume-rendered three-dimensional reconstruction image. Aneurysm was missed by algorithm, possibly because of small size (<3 mm) and location near skull base bone.

the vital factors in the clinical prediction of aneurysm rupture. Third, several false-positive findings were observed in areas with bony structures, veins, and vascular bifurcations and curvatures

and with calcified plaques. Most of these false-positive findings could easily be identified by the radiologists. Fourth, regarding the diagnostic performance assessment by using the wAFROC

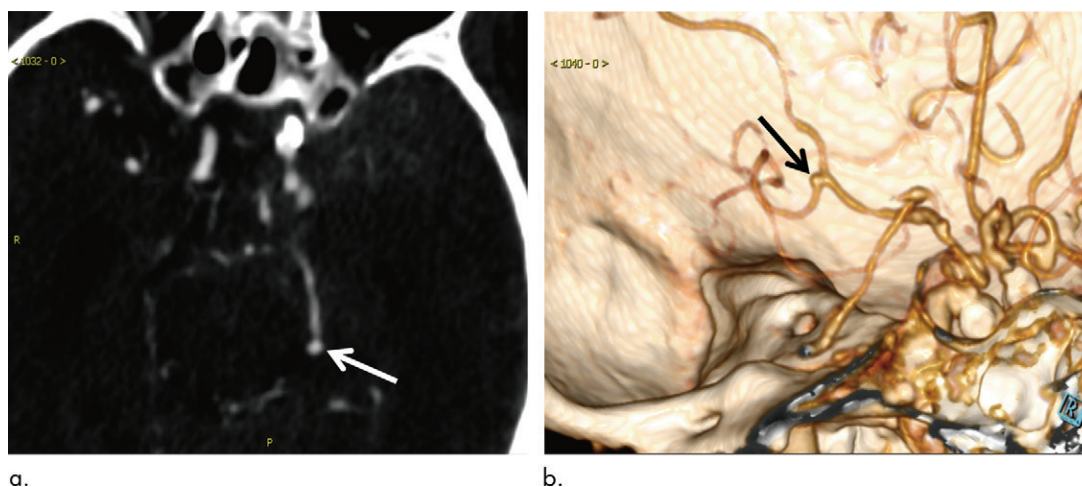


Figure 5: Images in 93-year-old woman with aneurysm 2 mm in maximum diameter located on left posterior cerebral artery (arrow). **(a)** Axial section head CT angiogram and **(b)** volume-rendered three-dimensional reconstruction image. Aneurysm was missed on initial report but was successfully detected with algorithm.

Table 3: Four Radiologists' Performance in Detection of Cerebral Aneurysms without and with Aid of Algorithm

Parameter	Without Algorithm	With Algorithm	Difference	P Value
Radiologist 1				
Area under wAFROC curve	0.58	0.61	0.03 (0.00, 0.06)	.049
Sensitivity per lesion (%)	62.86	86.67	23.81 (12.51, 35.11)	<.001
Sensitivity per case (%)	65.26	89.47	24.21 (12.82, 35.60)	<.001
Specificity per case (%)	97.14	85.71	−11.43 (−18.84, −4.02)	.003
Reading time (sec)	65.20	56.58	−8.62 (−14.08, −3.15)	<.001
Radiologist 2				
Area under wAFROC curve	0.60	0.62	0.02 (0.00, 0.04)	.03
Sensitivity per lesion (%)	75.70	90.65	14.95 (5.13, 24.77)	.004
Sensitivity per case (%)	80.81	94.95	14.14 (5.27, 23.02)	.002
Specificity per case (%)	98.02	86.14	−11.88 (−19.15, −4.62)	.002
Reading time (sec)	56.02	56.13	0.11 (−36.85, 37.07)	>.99
Radiologist 3				
Area under wAFROC curve	0.60	0.61	0.01 (−0.02, 0.04)	.62
Sensitivity per lesion (%)	85.15	87.13	1.98 (−7.55, 11.51)	.68
Sensitivity per case (%)	85.87	91.30	5.43 (−3.72, 14.59)	.25
Specificity per case (%)	97.22	96.30	−0.92 (−5.65, 3.80)	.70
Reading time (sec)	59.00	52.68	−6.32 (−14.02, 1.43)	.21
Radiologist 4				
Area under wAFROC curve	0.61	0.62	0.01 (−0.01, 0.01)	.36
Sensitivity per lesion (%)	91.26	93.20	1.94 (−5.36, 9.25)	.60
Sensitivity per case (%)	91.58	94.74	3.16 (−4.01, 10.32)	.39
Specificity per case (%)	91.43	95.24	3.81 (−2.92, 10.54)	.27
Reading time (sec)	31.90	32.20	0.30 (−5.00, 5.59)	>.99
Overall				
Area under wAFROC curve	0.60	0.61	0.01 (0.00, 0.03)	.03
Sensitivity per lesion (%)	79.09	88.94	9.85 (4.92, 14.79)	<.001
Sensitivity per case (%)	81.63	91.86	10.23 (5.48, 15.00)	<.001
Specificity per case (%)	95.94	90.93	−5.01 (−8.35, −1.68)	.003
Reading time (sec)	53.02	49.40	−3.62 (−9.85, 2.59)	.25

Note.—Data in parentheses are 95% CIs. wAFROC = weighted alternative free-response receiver operating characteristic.

method with equal weights, the clinical importance of each lesion in multiple-lesion CT angiograms was assumed to be equal to that of all other lesions, which might not exactly match the clinical standpoint. Fifth, the generalizability of the algorithm needs to be assessed on multicentric external data.

In future studies, segmentation of the cerebral aneurysms should be used to accurately describe the multidimensional aneurysm size and shape. In addition, the algorithm should be matured to improve its adaptability to each imaging system.

In conclusion, we introduced a highly sensitive deep learning-based algorithm for automated detection of cerebral aneurysms on CT angiography images. Radiologists' performance in detecting aneurysms improved with the aid of the algorithm, especially for less experienced radiologists.

Acknowledgments: We appreciate Xiaoming Yang, MD, PhD (Radiology, School of Medicine, University of Washington), for his kind assistance in editing and revising the manuscript and Hongwei Jiang, PhD (Epidemiology and Biostatistics, Tongji Medical College, Huazhong University of Science and Technology), for his assistance in statistical analysis.

Author contributions: Guarantors of integrity of entire study, X.M., C.H. O.A., Y.X., J.L., T.J., Changde Li, D.T., X. Liu, C.Z., X. Long; study concepts/study design or data acquisition or data analysis/interpretation, all authors; manuscript drafting or manuscript revision for important intellectual content, all authors; approval of final version of submitted manuscript, all authors; agrees to ensure any questions related to the work are appropriately resolved, all authors; literature research, J.Y.C.H., O.A., Y.X., D.T., X. Liu, C.Z., Cixing Li; clinical studies, X.M., O.A., J.L., T.J., Changde Li, D.T., C.Z., X. Long; experimental studies, J.Y., C.H., Y.X., J.L., T.J., Changde Li, D.T., X. Liu, C.Z., Cixing Li; statistical analysis, J.Y., C.H., Y.X., D.T., X. Liu, C.Z., Cixing Li; and manuscript editing, J.Y., X.M., C.H., O.A., Y.X., D.T., C.Z., X. Long.

Disclosures of Conflicts of Interest: J.Y. disclosed no relevant relationships. M.X. disclosed no relevant relationships. C.H. disclosed no relevant relationships. O.A. disclosed no relevant relationships. Y.X. disclosed no relevant relationships. J.L. disclosed no relevant relationships. T.J. disclosed no relevant relationships. Changde Li disclosed no relevant relationships. D.T. disclosed no relevant relationships. X. Liu disclosed no relevant relationships. C.Z. disclosed no relevant relationships. Cixing Li disclosed no relevant relationships. X. Long disclosed no relevant relationships.

References

- van Gijn J, Kerr RS, Rinkel GJ. Subarachnoid haemorrhage. *Lancet* 2007; 369(9558):306–318.
- Westerlaan HE, van Dijk JM, Jansen-van der Weide MC, et al. Intracranial aneurysms in patients with subarachnoid hemorrhage: CT angiography as a primary examination tool for diagnosis—systematic review and meta-analysis. *Radiology* 2011;258(1):134–145.
- Ingall T, Asplund K, Mähönen M, Bonita R. A multinational comparison of subarachnoid hemorrhage epidemiology in the WHO MONICA stroke study. *Stroke* 2000;31(5):1054–1061.
- Hop JW, Rinkel GJ, Algra A, van Gijn J. Case-fatality rates and functional outcome after subarachnoid hemorrhage: a systematic review. *Stroke* 1997;28(3):660–664.
- UCAS Japan Investigators; Morita A, Kirino T, et al. The natural course of unruptured cerebral aneurysms in a Japanese cohort. *N Engl J Med* 2012;366(26):2474–2482.
- Park A, Chute C, Rajpurkar P, et al. Deep Learning-Assisted Diagnosis of Cerebral Aneurysms Using the HeadXNet Model. *JAMA Netw Open* 2019;2(6):e195600.
- Philipp LR, McCracken DJ, McCracken CE, et al. Comparison between CTA and digital subtraction angiography in the diagnosis of ruptured aneurysms. *Neurosurgery* 2017;80(5):769–777.
- Yoon NK, McNally S, Taussky P, Park MS. Imaging of cerebral aneurysms: a clinical perspective. *Neurovasc Imaging* 2016;2(1):6.
- Hosny A, Parmar C, Quackenbush J, Schwartz LH, Aerts HJWL. Artificial intelligence in radiology. *Nat Rev Cancer* 2018;18(8):500–510.
- Larson DB, Chen MC, Lungren MP, et al. Performance of a deep-learning neural network model in assessing skeletal maturity on pediatric hand radiographs. *Radiology* 2017;287(1):313–322.
- Lakhani P, Sundaram B. Deep learning at chest radiography: automated classification of pulmonary tuberculosis by using convolutional neural networks. *Radiology* 2017;284(2):574–582.
- Ueda D, Yamamoto A, Nishimori M, et al. Deep learning for MR angiography: automated detection of cerebral aneurysms. *Radiology* 2019;290(1):187–194.
- Arbabshirani MR, Fornwalt BK, Mongelluzzo GJ, et al. Advanced machine learning in action: identification of intracranial hemorrhage on computed tomography scans of the head with clinical workflow integration. *NPJ Digit Med* 2018;1(1):9.
- Hamidian S, Sahiner B, Petrick N, Pezeshk A. 3D Convolutional Neural Network for Automatic Detection of Lung Nodules in Chest CT. *Proc SPIE Int Soc Opt Eng* 2017;10134:1013409.
- Liu K, Li Q, Ma J, et al. Evaluating a Fully Automated Pulmonary Nodule Detection Approach and Its Impact on Radiologist Performance. *Radiol Artif Intell* 2019;1(3):e180084.
- Titano JJ, Badgeley M, Schefflein J, et al. Automated deep-neural-network surveillance of cranial images for acute neurologic events. *Nat Med* 2018;24(9):1337–1341.
- Liao F, Liang M, Li Z, Hu X, Song S. Evaluate the Malignancy of Pulmonary Nodules Using the 3-D Deep Leaky Noisy-OR Network. *IEEE Trans Neural Netw Learn Syst* 2019;30(11):3484–3495.
- Woo S, Park J, Lee JY, Kweon IS. CBAM: Convolutional Block Attention Module. In: Ferrari V, Hebert M, Sminchisescu C, Weiss Y, eds. *Computer Vision – ECCV 2018*. ECCV 2018. Lecture Notes in Computer Science, vol 11211. Cham, Switzerland: Springer, 2018; 3–19.
- He K, Zhang X, Ren S, Sun J. Deep Residual Learning for Image Recognition. In: 2016 IEEE Conference on Computer Vision and Pattern Recognition (CVPR), Las Vegas, NV, June 27–30, 2016. Piscataway, NJ: IEEE, 2016.
- Gu Z, Cheng J, Fu H, et al. CE-Net: Context Encoder Network for 2D Medical Image Segmentation. *IEEE Trans Med Imaging* 2019;38(10):2281–2292.
- Chakraborty DP. A brief history of free-response receiver operating characteristic paradigm data analysis. *Acad Radiol* 2013;20(7):915–919.
- Sichtermann T, Faron A, Sijben R, Teichert N, Freiherr J, Wiesmann M. Deep Learning-Based Detection of Intracranial Aneurysms in 3D TOF-MRA. *AJNR Am J Neuroradiol* 2019;40(1):25–32.
- Nakao T, Hanaoka S, Nomura Y, et al. Deep neural network-based computer-assisted detection of cerebral aneurysms in MR angiography. *J Magn Reson Imaging* 2018;47(4):948–953.
- Vaseemahamed M, Ravishankar M. Automated System for Detection of Cerebral Aneurysms in Medical CTA Images. In: Satapathy S, Biswal B, Udgata S, Mandal J, eds. *Proceedings of the 3rd International Conference on Frontiers of Intelligent Computing: Theory and Applications (FICTA) 2014*. Advances in Intelligent Systems and Computing, vol 328. Cham, Switzerland: Springer, 2015; 537–543.
- Miki S, Hayashi N, Masutani Y, et al. Computer-Assisted Detection of Cerebral Aneurysms in MR Angiography in a Routine Image-Reading Environment: Effects on Diagnosis by Radiologists. *AJNR Am J Neuroradiol* 2016;37(6):1038–1043.